

Due to the large detection distance, sparse distributions of our unobtrusive low-cost beacons is sufficient to augment wide areas for autonomous vehicle deployments or other robotic applications. For example, our detection distance is three times greater than the typical distance between light poles in urban areas in Germany. Our contributions are summarized as follows:

- We propose a simple and robust approach for infrastructure-based keypoints based on sparsely distributed infrared beacons.
- We describe the hardware and protocol design and image processing pipeline in detail.
- We provide a proof-of-concept evaluation for a long-range outdoor scenario for both day and night.

II. RELATED WORK

GNSS approaches such as GPS or Galileo use satellite signals to determine the current position. While GPS achieves meter accuracy [2], performance can be improved through the use of differential GPS (DGPS) or real-time kinematic (RTK) solutions, which use base-stations with known location to improve positioning accuracy [3]. The reliability problem remains in urban environments or tunnels, where signals can be reflected or blocked entirely, culminating in reduced accuracy or inability to localize. To overcome situations with degraded GNSS availability, inertial measurement units (IMUs) have been used to estimate the vehicle position relative to an initial position. For example, Zhang et al. [4] improve raw GPS performance through fusion with an IMU, but the accumulated root mean square positioning error after 408 m is at 7.4 m, which is too high for automated driving.

Camera-based techniques have been investigated in numerous publications [5]–[9]. Often, these techniques rely on heuristic feature points, which are embedded in a map and matched with features extracted from live camera images for localization. In [10] Sattler et al. benchmark various approaches under changing environment conditions and conclude *‘that long-term localization is far from solved’*. Problems arise from feature detection and matching with corresponding map features as the scene appearance changes over time. Frequent map updates and semantic information may accommodate for long-term changes [11], [12], but performance issues under different lighting and weather situations remain.

Infrastructure-based approaches try to alleviate recognition problems of heuristic features by purposely placing hand-crafted features or devices in the environment. We first present related work for indoor systems and then discuss prior work for outdoor applications.

Li et al. propose Epsilon, an indoor positioning system that uses regular LED lamps [13] and that achieves sub-meter accuracy indoor. The authors of [14] use infrared LEDs placed on walls, which are detected using a camera system, allowing for mobile robot localization. To simplify detection, an optical low-pass filter is used in front of the camera, which blocks visible light. Different to our work, the LEDs do not

communicate an identifier and are not distinguishable. Fiducial tags such as arUco [15] and AprilTags [16] are purposely designed for robust recognition. Due to their passive nature, they are difficult to detect and identify at long-range and require high density. In contrast, our we try to minimize the number of beacons required, potentially rendering the idea economically feasible and avoiding environmental clutter.

The Vehicle Information and Communication System (VICS) in Japan consists of over 56.000 infrared transceivers that are used for traffic monitoring and traffic information purposes. The beacons are mounted above the road, have a communication range of 3.5 m. In [17], the authors were able to extend the communication range to 6 m. Our proposed system is related to the Visible Light Communication (VLC) domain [18], for which we will now present related work. In [19] the authors modulate traffic light intensities and capture and decode the transmitted signal using a camera. The authors do not test their system in motion and traffic lights are too sparsely distributed to be used for localization in wider areas. The authors of [20] also investigate the use of traffic lights as communication channels and achieve transmission rates of multiple Mbit/s. The same authors design a system using a LED-based transmitter capable of high-speed transmissions, but rely on an expensive high-speed camera and much larger beacons [21], [22]. In [23], Liu et al. propose an outdoor localization system incorporating LEDs in traffic lights and visible light beacons. In contrast to our work, the use of optical band-pass filters was not investigated and no outdoor evaluation was conducted. Kim et al. propose a VLC system for localization but the demonstration and evaluation is carried out only in simulation [24].

The authors of [1] propose coded beacons (CoBe) using infrared LEDs for localization and object tracking and obtain convincing results. This contribution differs in various aspects from CoBE. First, we demonstrate the effectiveness of our system in long range outdoor scenarios, while the performance of CoBE is only investigated indoors. Second, we make use of a bandpass filter, instead of a regular high-pass filter as used by CoBE. We found that replacing a bandpass filter with a high-pass filter causes significantly more noise from sun light. This makes beacon detection and identification at long ranges more error prone. Third, our line code ensures that beacons are never completely turned off. We found this to be instrumental for tracking beacons when the vehicle moves at higher speeds. Since our beacons are attached to light poles, they cluster closely at long ranges, which increases ambiguity and tracking complexity if they are off for multiple frames. Additionally, our approach also significantly differs in the decoding scheme and hardware setup.

III. SYSTEM DESIGN

The underlying idea of this work is to embed active visual beacons into the infrastructure that act as long-term stable, unambiguous, and easily detectable features to facilitate long-term stable vehicle localization in urban environments under changing environment conditions. Our

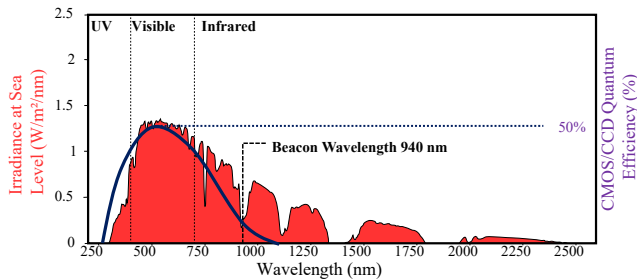


Fig. 2. Intensity of sunlight across the wavelength spectrum decreases in the infrared and ultra-violet regions. The selected LED and band-pass combination exploits the intensity drop at 940 nm, where sunlight intensity is low but still detectable for off-the-shelf CMOS/CCD cameras sensors.

privacy-preserving beacons actively communicate a beacon identifier using infrared light. Thus, their visibility is not dependent on environmental conditions and external light sources, as would be the case with traffic signs or passive QR codes. Furthermore, our system is designed to increase the signal-to-noise ratio, i.e., the visibility of the infrared beacons in contrast to other elements of the environment at the camera sensor. This is achieved by restricting the wavelengths of light that reach the camera sensor to a small window around the wavelength emitted by our beacons through the use of a band-pass filter.

A. Hardware Design

Signal-to-Noise Ratio: During the daytime, the most dominant cause of interference is sunlight. As Fig. 2 shows, the sun as an idealized black-body radiation source emits light across the full wavelength spectrum at varying intensity levels [25]. The sun radiates light with the highest intensity in the human visible spectrum and intensity drops for ultra-violet and infrared light. Ideally, the beacon wavelength would be as far as possible in the infrared spectrum to avoid the beacon signal to overlap with natural sunlight. Due to physical limitations imposed by the photoelectric effect, quantum efficiency for common, silicon-based camera sensors drops to zero at 1.12 eV photon energy, which corresponds to 1100 nm light wavelength. Infrared cameras can overcome this limitation through the use of different sensor principles, but are very expensive and are therefore not considered. However, there are a few characteristic drops in sunlight intensity for specific wavelengths caused by interference with molecules in the atmosphere. The drop at 940 nm is particularly strong and is the furthest into the infrared spectrum that is still detectable for regular camera sensors.

Beacon and Camera Prototype: Fig. 3 depicts our proof-of-concept beacons that are made up of 48 LEDs at 940 nm wavelength and measure 6 cm \times 6 cm. In order to allow for investigating different patterns, the LEDs are divided into 16 groups with 3 LEDs each. The monochrome camera for beacon detection has a resolution of 1600 px \times 1200 px and is equipped with a band-pass filter for 950 nm wavelength with a full-width-at-half-maximum value of 50 nm. The

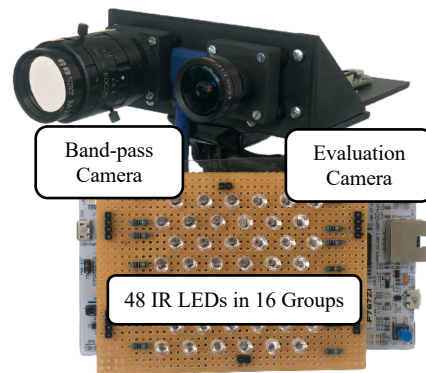


Fig. 3. Our prototype beacon and camera system consisting of a camera with optical band-pass and the evaluation camera.

camera records images at 100 Hz. To eliminate remaining 940 nm sunlight, the beacon detection camera uses a low exposure time of 100 μ s. As depicted in Fig. 5, most of the environment is removed by the filter and the beacons are clearly visible at nighttime and also against direct sunlight during the daytime. Most of the surrounding environment is removed from the image, thereby dramatically increasing the signal-to-noise ratio and easing beacon detection.

B. Optical Communication Channel

Preliminary considerations: We considered two approaches for designing the communication channel between beacon and camera. In a pure spatial encoding approach, each beacon displays a unique pattern for identification (e.g., QR codes). Global identifier uniqueness would not be required as long as it is unique for a sufficiently large local neighborhood of beacons. As a result, beacons can potentially be identified from a single camera image instead of having to track and reconstruct the signal over multiple images. For this approach, identification of individual LEDs or groups of LEDs is required, which becomes infeasible after a few meters with a 6 cm \times 6 cm beacon size (see Fig. 5). This approach may be feasible with extreme camera resolutions or significantly larger beacons—options we discarded for practical considerations.

Linecode: We choose a mixture of time and spatial encoding, where the identifier is transmitted through the alternation between simple patterns over time. An intuitive encoding scheme is turning the beacon on and off in order to transmit 1 or 0. Due to the large displacements during the off phase, tracking at a vehicle speed of 30 km/s has proven difficult in experiments — especially with multiple beacons. Instead, we use the diagonal symbols depicted in Fig. 4

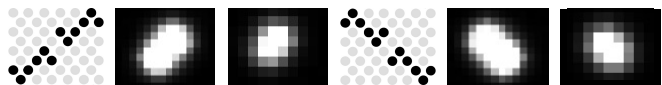


Fig. 4. A diagonal pattern is used as symbols for data transmission with examples at 25 m and 50 m as seen by the band-pass camera.

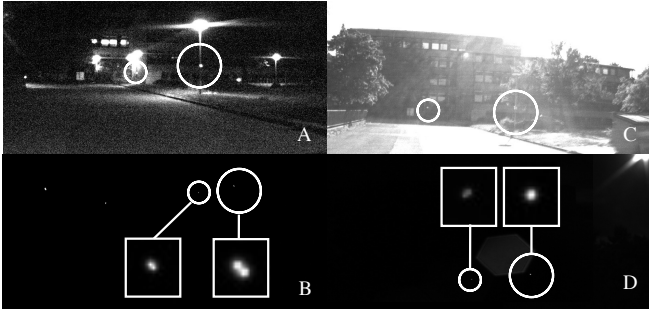


Fig. 5. Image captured at night (A,B) and against direct sunlight (C,D) with clearly visible beacons in the corresponding band-pass filtered images. Rectangles indicate magnifications of the circled image areas.

to implement a non-return-to-zero line code. Depending on diagonal orientation, 1 or 0 is represented. The figure shows the symbols at 25 m and 50 m as captured by the camera. Here it becomes obvious that identifying individual LED groups is not tractable for a pure spatial domain encoding. The chosen approach has the advantage that the beacons are always active, which eases tracking and subsequently signal reconstruction.

Beacon identifier: A 12-Bit-Code is assigned to every beacon, which is transmitted in an endless loop using the two previously introduced symbols, see Fig. 4. We do not use a synchronization symbol. Ambiguities arise if codes are chosen unconstrained, e.g. 00110011 and 11001100 generate the same signal if repeated indefinitely. Therefore, we use prefix-free codes that are generated through ambiguity testing of all cyclic shifts for all 2^{12} possible identifiers. The camera records an image every 10 ms while the beacon displays each bit for 70 ms, which allows for oversampling and more robust signal reconstruction. Transmission of the full 12-bit beacon identifier takes 0.84 s.

C. Image Processing

We will now describe the image processing pipeline used for beacon detection and identification. The processing pipeline generates image patches that potentially contain beacons. Candidates are tracked across multiple images and the signal is reconstructed.

Beacon Detection: The beacon detection stage first operates on binarized images for filtering purposes, but uses grayscale images for subsequent stages. We first generate a set of proposal image patches that contain potential beacons and filter the proposals based on reference image comparison. First, the 8-bit grayscale image I_G is converted to a binary image I_B by setting pixel intensities lower than 5 to zero, and pixel values above 5 to 1. Next, a set of contiguous areas are extracted from the camera image using morphological operations as beacon proposals $P = \{(x_1, y_1, w_1, h_1), \dots, (x_n, y_n, w_n, h_n)\}$. Each area is described through its bounding box width, height and location in the camera image.

As beacons have a fixed size, the maximum and minimum area occupied in the camera image depends only on the

distance to the camera. The upper and lower bounds can be determined analytically using the pinhole camera model. In theory, a beacon at 60 m occupies only $2 \text{ px} \times 2 \text{ px}$ according to the pinhole model. However, due to the fact that neighboring pixels are also illuminated, the beacon orientation is still distinguishable at well over 100 m (see Section IV). The proposals P are filtered based on these limits such that both large-scale artifacts and individual white pixels are excluded. The set of proposals is refined to P_R based on proposal area: $P_R = \{(x, y, w, h) \in P \mid wh \in [3, 400]\}$. For distant beacons, individual pixels of low intensity have been removed by thresholding, but the decoder is still able to determine the orientation correctly in the grayscale image I_G .

The final detection step uses shape matching to compare the proposals with a reference image I_R . To this end, we compute Hu-moments for each beacon $b \in P_R$ in the original grayscale image I_G , which are translation, rotation and scale-invariant [26]. Image moments of order $i + j$ are defined as follows:

$$\mu_{ij} = \sum_x \sum_y (x - \bar{x})^i (y - \bar{y})^j I_G(x, y) \quad (1)$$

with \bar{x} and \bar{y} being the centroids in each dimension:

$$\bar{x} = \frac{\sum_x \sum_y x I_G(x, y)}{\sum_x \sum_y I_G(x, y)} \quad (2)$$

$$\bar{y} = \frac{\sum_x \sum_y y I_G(x, y)}{\sum_x \sum_y I_G(x, y)} \quad (3)$$

Scale invariant moments are then obtained through normalization as:

$$\eta_{ij} = \frac{\mu_{ij}}{\mu_{00}^{\frac{i+j}{2}+1}} \quad (4)$$

The seven rotational invariant Hu-moments c_1, \dots, c_7 can then be defined using η_{ij} . For example $c_1 = \eta_{20} + \eta_{02}$ and $c_2 = (\eta_{20} - \eta_{02})^2 + 4\eta_{11}^2$. A complete list of all moment definitions is provided in [26]. The distance between I_R and a proposal patch I_P extracted from I_G is then computed on the basis of respective Hu-moments:

$$D(I_P, I_R) = \sum_{i=1}^7 \left| \frac{1}{\text{sgn}(c_i^P) \log c_i^P} - \frac{1}{\text{sgn}(c_i^R) \log c_i^R} \right| \quad (5)$$

Proposals for which $D(I_P, I_R) < 0.2$ holds are regarded as detections $d \in D$ and are passed to the tracker.

Tracking: Due to the high frame rate of 100 Hz, we assume only small shifts of the beacon position between consecutive images. Input to this stage are tracked beacons from previous images denoted as tracks $T = \{t_1, \dots, t_l\}$ and detections for the current camera image $D = \{d_1, \dots, d_k\}$. We compute a distance matrix for each detection and track combination based on the euclidean distance of bounding box centroids as follows: We follow a greedy approach and associate tracks and detections starting with the smallest distance up to a maximum distance threshold. A new track is created for all detections that can not be matched to any existing track,

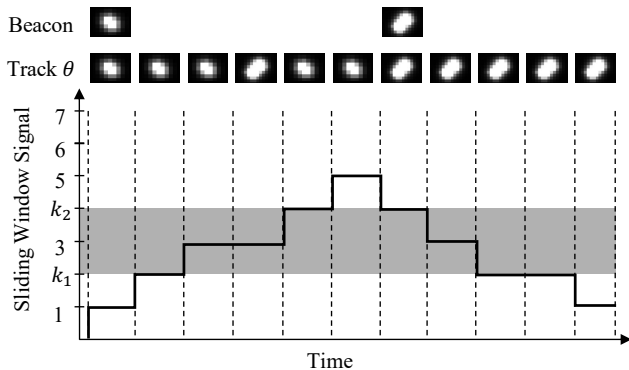


Fig. 6. Signal reconstruction uses a sliding window summation over the previous orientation estimates. A Schmitt trigger evaluates the sliding window signal.

either due to exceeding the maximum distance or because all other tracks have been matched. Tracks are discarded if they are not matched to a detection for more than 30 frames. **Signal Reconstruction:** The decoder attempts to recover the identifier for each track. For this, the orientation of the symbol is determined based on the central image moments:

$$\theta = \frac{1}{2} \arctan \left(\frac{2\mu_{11}}{\mu_{20} - \mu_{02}} \right) \quad (6)$$

Orientations are mapped to 1 if $\theta > 0$ and to 0 otherwise. The decoder is designed to make use of the oversampled symbol display, i.e., 10 ms time between camera images and 70 ms display time for a single bit. For each track, a sliding window sums up the last seven estimated bit values (c.f. Eq. 6). As depicted in Figure 6, the sliding window produces a signal n that is input to a Schmitt trigger, with threshold values $k_1 = 2$ and $k_2 = 4$. If the sum exceeds k_2 , the beacon signal is interpreted as 1, and if it falls below k_1 as 0. Whenever a signal level change has been detected, a single bit is appended to the decoded identifier of the track corresponding to the Schmitt trigger state and the time of signal change is stored. The decoder also handles repetitions of the same symbol, as the time to sample the Schmitt trigger is derived from the known beacon frequency. Each track t_i generates a bit sequence that can be matched to a known list of beacon identifiers.

IV. EXPERIMENTS & RESULTS

The following experiments are conducted on a straight road. As displayed in Fig. 7, we have mounted beacons B_1 , B_2 and B_3 on light poles that are on average 40 m apart. Fig. 7 shows the distance of each beacon to the starting point S , with B_1 being the furthest away at 150 m. A video that demonstrates the experiments is available in [27].

A. Standstill Experiment

This experiment intends to determine the system performance when the vehicle is not moving. For this purpose, only beacon B_1 is activated and we have parked our test vehicle 40 m, 60 m, 80 m, 100 m, and 120 m away from B_1 .

TABLE I

PERFORMANCE AT VARIOUS DISTANCES DURING STANDSTILL

Metric	40 m	60 m	80 m	100 m	120 m
Frames	2264	2279	2277	2278	2276
Detections	2264	2279	2277	2278	2269
Tracks	1	1	1	1	1
Bits Decoded	263	265	263	261	271
Error Bits	0	0	0	0	104

We investigate the ability of the system to correctly decode the identifier transmitted by the beacon. This experiment evaluates the end-to-end performance of the system since a correctly decoded beacon identifier requires all stages of the processing pipeline to function correctly. All recordings for this experiment have been recorded during daytime.

The outcome of this experiment is summarized in Table I. Although the experiment was conducted in daylight, no detections and thus tracks were generated other than the one corresponding to the beacon for all distances. The total number of bits decoded corresponds to the length of the bit-string that is generated by the signal reconstruction stage.

We count all occurrences of the known beacon identifier in the decoded bit-string. The first and last bits are also considered correct if they are a part of the true identifier. All remaining bits are considered error bits. For example, if we decode 11001000010011001010001001100100001, then 110010X1X0001 results after replacing all occurrences of $id(B_1) = 000100110010$ with X. Since 110010 and 0001 are part of $id(B_1)$, we count the number of correctly decoded bits as 34 and the number of error bits as 1.

The results show that the system correctly derives the beacon identifier up to a distance of 100 m error-free. We see that the system is also able to detect and track the beacon at a distance of 120 m. The fact that there are less detections than frames indicates that the detector fails to generate beacon candidates, with a negative impact on the decoded bit sequence. Although we were still able to find $id(B_1)$ in the decoded bit string multiple times at 120 m, we see that errors start to occur. For practical applications,

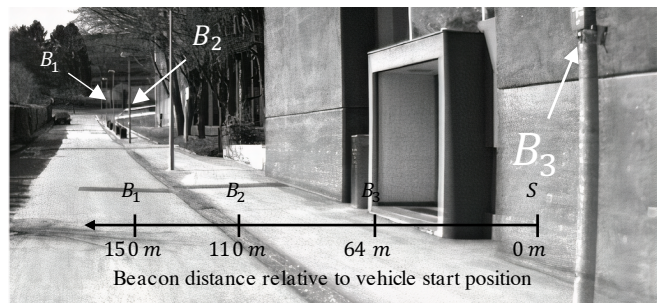


Fig. 7. Our experiment consists of beacons B_1 , B_2 and B_3 mounted 40 m apart on average. The vehicle starts 150 m away from B_1 .

TABLE II

EVALUATION AT DAYTIME D_i AND NIGHTTIME N_i . THE VEHICLE POSITION UPON FIRST AND LAST CORRECT IDENTIFIER RECOGNITION IS REPORTED. BEACONS ARE DETECTED OVER A DISTANCE OF MORE THAN 100 m.

	D_1	D_2	D_3	D_4	Avg.	N_1	N_2	N_3	N_4	Avg.
Frames	2940	2771	2723	2626	2765.0	2739	2678	2643	2739	2699.75
Detections	5247	5026	5097	4935	5076.25	4958	4895	4667	4736	4814.0
Tracks	10	9	12	11	10.5	5	5	8	7	6.25
B_1 Tracks	1	1	1	1	1.0	1	2	1	1	1.25
B_1 First Recognition	50.9 m	51.8 m	50.2 m	51.4 m	51.07 m	14.5 m	18.5 m	64.6 m	45.0 m	35.65 m
B_1 Last Recognition	145.0 m	145.1 m	149.9 m	145.3 m	146.32 m	148.2 m	148.0 m	148.0 m	148.5 m	148.18 m
B_1 Bits Decoded	213	217	231	194	213.75	279	263	172	209	230.75
B_1 Error Bits	33	49	75	17	43.5	51	71	11	29	40.5
B_2 Tracks	1	1	1	1	1.0	1	1	1	1	1.0
B_2 First Recognition	4.0 m	5.5 m	6.3 m	7.7 m	5.88 m	6.8 m	6.5 m	8.2 m	10.0 m	7.88 m
B_2 Last Recognition	105.6 m	105.5 m	105.2 m	105.0 m	105.33 m	105.9 m	105.9 m	105.5 m	105.4 m	105.68 m
B_2 Bits Decoded	234	213	216	211	218.5	223	221	217	221	220.5
B_2 Error Bits	6	7	18	10	10.25	10	11	14	29	16.0
B_3 Tracks	1	1	1	1	1.0	1	1	1	1	1.0
B_3 First Recognition	4.8 m	7.2 m	8.4 m	5.4 m	6.45 m	7.1 m	5.7 m	8.6 m	7.1 m	7.12 m
B_3 Last Recognition	62.1 m	62.4 m	61.7 m	62.1 m	62.07 m	63.5 m	63.8 m	63.0 m	63.0 m	63.33 m
B_3 Bits Decoded	151	132	131	131	136.25	141	142	133	141	139.25
B_3 Error Bits	0	5	0	20	6.25	12	5	4	12	8.25

this might still be sufficient. While the position of B_1 in the camera image is crucial for ego-pose estimation, querying the geographical location of the beacon using the identifier only has to be done once.

B. Driving Experiment

This experiment determines the ability of the system to detect and identify the beacons while driving. The vehicle accelerates from a standstill at position S to 8.3 m/s and drives towards the end of the road until it passes B_1 . All three beacons are active with $id(B_2) = 010100100110$ and $id(B_3) = 000101010100$. We have conducted eight runs of this experiment, four during daytime and four at nighttime.

The results for this experiment are shown in Table II. We report the total number of frames, detections, tracks as well as total bits decoded for each recording. The number of detections per run appear large, but it is less than three beacons per frame. This is expected, as B_2 and B_3 leave the field of view and B_1 is picked up only after 50 m. Furthermore, we report the number of tracks for each beacon where the generated decoder bit sequence contains the correct beacon identifier. In each run, only one track generates the correct identifier per beacon, with an exception of run N_2 . In N_2 , beacon B_1 is recognized very early. This early generated track is discarded as the detector fails to find B_1 . Later on, B_1 is picked up at the same distance as in the other experiments.

We also show the vehicle position (cf. Fig. 7) of the first and last recognition of the full beacon identifier. B_3 and B_2 are identified within the 100 m recognition range observed during the standstill experiment. The detection distance is

non-zero, as the vehicle is in motion and the transmission of the 12-bit identifier takes 0.84 s. At 8.3 m/s, the vehicle drives 6.9 m during a complete identifier transmission. The observed numbers are slightly lower than in the standstill experiment.

Table II also shows the correct and incorrect bits in the decoded bit string as defined in the standstill experiment. Here, we can observe a higher number of error bits. We found that in many cases the errors occur at the end of track lifetime. As beacons leave the field of view, bit are mistakenly appended as the decoder assumes symbol repetition.

The performance of the system does not differ significantly during nighttime or daytime, which becomes clear when comparing decoding errors. This might be attributed to normalization of the camera image achieved by the band-pass filter. Due to the absence of light sources at 940 nm wavelength, the number of detections and thus the number of tracks is slightly lower at nighttime. It is noteworthy that $id(B_1)$ is recognized on average 15.4 m earlier at nighttime in comparison to daytime. The greater recognition distance might be attributed to less noisy detections and therefore more robust template matching in the detector.

V. CONCLUSION & FUTURE WORK

We have presented an approach for infrastructure-based localization using infrared beacons and a band-pass filtered camera system. The system setup and underlying design considerations have been elaborated. We have described our image processing pipeline that uses traditional computer vision techniques. Our experiments demonstrate the ability of the system to detect, track and identify our beacons

independent of light conditions at long ranges. As our detection range is greater than the typical distance between light poles in urban areas, the obtrusive and costly construction of new infrastructure is not required. The use of infrared light increases signal-to-noise ratio and is invisible to the human eye. Our contribution can be regarded as a proof-of-concept but more large-scale investigations have to be carried out. These experiments will also investigate the final positioning performance achieved. Additionally, we plan to investigate alternative beacon patterns, as our beacon prototype allows to display up to 65,535 different symbols.

REFERENCES

- [1] R. Rabinovich, I. Jubran, A. Wetzler, and R. Kimmel, "CoBe - coded beacons for localization, object tracking, and SLAM augmentation," in *2020 IEEE 16th International Conference on Automation Science and Engineering (CASE)*, pp. 1367–1374, 2020.
- [2] H. Tan and J. Huang, "DGPS-based vehicle-to-vehicle cooperative collision warning: Engineering feasibility viewpoints," *IEEE Transactions on Intelligent Transportation Systems*, vol. 7, no. 4, pp. 415–428.
- [3] S. Kuutti, S. Fallah, K. Katsaros, M. Dianati, F. McCullough, and A. Mouzakitis, "A survey of the state-of-the-art localization techniques and their potentials for autonomous vehicle applications," *IEEE Internet of Things Journal*, vol. 5, no. 2, pp. 829–846, 2018.
- [4] F. Zhang, H. Stähle, G. Chen, C. C. C. Simon, C. Buckl, and A. Knoll, "A sensor fusion approach for localization with cumulative error elimination," in *2012 IEEE International Conference on Multisensor Fusion and Integration for Intelligent Systems (MFI)*, pp. 1–6, 2012.
- [5] Y. Li, N. Snavely, and D. P. Huttenlocher, "Location recognition using prioritized feature matching," in *Computer Vision – ECCV 2010* (K. Daniilidis, P. Maragos, and N. Paragios, eds.), Lecture Notes in Computer Science, pp. 791–804, Springer, 2010.
- [6] T. Sattler, M. Havlena, F. Radenovic, K. Schindler, and M. Pollefeys, "Hyperpoints and fine vocabularies for large-scale location recognition," in *Proceedings of the IEEE International Conference on Computer Vision*, pp. 2102–2110, 2015.
- [7] A. Torii, R. Arandjelovic, J. Sivic, M. Okutomi, and T. Pajdla, "24/7 place recognition by view synthesis," in *Proceedings of the IEEE Conference on Computer Vision and Pattern Recognition*, pp. 1808–1817, 2015.
- [8] H. Taira, M. Okutomi, T. Sattler, M. Cimpoi, M. Pollefeys, J. Sivic, T. Pajdla, and A. Torii, "InLoc: Indoor visual localization with dense matching and view synthesis," in *Proceedings of the IEEE Conference on Computer Vision and Pattern Recognition*, pp. 7199–7209, 2018.
- [9] E. Brachmann and C. Rother, "Visual Camera Re-Localization from RGB and RGB-D Images Using DSAC," *IEEE Transactions on Pattern Analysis and Machine Intelligence*, pp. 1–1, 2021. Conference Name: IEEE Transactions on Pattern Analysis and Machine Intelligence.
- [10] T. Sattler, W. Maddern, C. Toft, A. Torii, L. Hammarstrand, E. Stenborg, D. Safari, M. Okutomi, M. Pollefeys, J. Sivic, F. Kahl, and T. Pajdla, "Benchmarking 6dof outdoor visual localization in changing conditions," in *Proceedings of the IEEE Conference on Computer Vision and Pattern Recognition*, pp. 8601–8610, 2018.
- [11] J. L. Schönberger, M. Pollefeys, A. Geiger, and T. Sattler, "Semantic visual localization," in *2018 IEEE/CVF Conference on Computer Vision and Pattern Recognition*, pp. 6896–6906, 2018.
- [12] Z. Xiao, K. Jiang, S. Xie, T. Wen, C. Yu, and D. Yang, "Monocular vehicle self-localization method based on compact semantic map*," in *2018 21st International Conference on Intelligent Transportation Systems (ITSC)*, p. 3083–3090, Nov 2018.
- [13] L. Li, P. Hu, C. Peng, G. Shen, and F. Zhao, "Epsilon: A visible light based positioning system," in *11th USENIX Symposium on Networked Systems Design and Implementation (NSDI 14)*, pp. 331–343, 2014.
- [14] S. Hijikata, K. Terabayashi, and K. Umeda, "A simple indoor self-localization system using infrared leds," in *2009 Sixth International Conference on Networked Sensing Systems (INSS)*, 2009.
- [15] S. Garrido-Jurado, R. Muñoz-Salinas, F. Madrid-Cuevas, and R. Medina-Carnicer, "Generation of fiducial marker dictionaries using mixed integer linear programming," *Pattern Recognition*, vol. 51, 2015.
- [16] E. Olson, "AprilTag: A robust and flexible visual fiducial system," in *2011 IEEE International Conference on Robotics and Automation*, pp. 3400–3407, 2011.
- [17] K. Hayama, H. Shiranaga, K. Miyake, and Y. Taniguchi, "Advanced infrared beacon with increased communication capacity," *SEI technical review*, vol. 185, pp. 72–76, 2014.
- [18] T. Yamazato, "Overview of visible light communications with emphasis on image sensor communications," in *2017 23rd Asia-Pacific Conference on Communications (APCC)*, pp. 1–6, 2017.
- [19] E. Eso, Z. Ghassemlooy, S. Zvanovec, A. Gholami, A. Burton, N. B. Hassan, and O. I. Younus, "Experimental demonstration of vehicle to road side infrastructure visible light communications," in *2019 2nd West Asian Colloquium on Optical Wireless Communications (WACOWC)*, pp. 85–89, 2019.
- [20] T. Yamazato, I. Takai, H. Okada, T. Fujii, T. Yendo, S. Arai, M. Andoh, T. Harada, K. Yasutomi, K. Kagawa, and S. Kawahito, "Image-sensor-based visible light communication for automotive applications," *IEEE Communications Magazine*, vol. 52, no. 7, pp. 88–97, 2014.
- [21] T. Nagura, T. Yamazato, M. Katayama, T. Yendo, T. Fujii, and H. Okada, "Improved decoding methods of visible light communication system for ITS using LED array and high-speed camera," in *2010 IEEE 71st Vehicular Technology Conference*, pp. 1–5, 2010.
- [22] T. Nagura, T. Yamazato, M. Katayama, T. Yendo, T. Fujii, and H. Okada, "Tracking an LED array transmitter for visible light communications in the driving situation," in *2010 7th International Symposium on Wireless Communication Systems*, pp. 765–769, 2010.
- [23] Hugh Sing Liu and G. Pang, "Positioning beacon system using digital camera and leds," *IEEE Transactions on Vehicular Technology*, vol. 52, no. 2, pp. 406–419, 2003.
- [24] B. W. Kim and S. Jung, "Vehicle positioning scheme using v2v and v2i visible light communications," in *2016 IEEE 83rd Vehicular Technology Conference (VTC Spring)*, pp. 1–5, 2016.
- [25] M. Iqbal, *An Introduction To Solar Radiation*. Elsevier.
- [26] Ming-Kuei Hu, "Visual pattern recognition by moment invariants," *IRE Transactions on Information Theory*, vol. 8, no. 2, pp. 179–187, 1962.
- [27] "Outdoor Recognition Performance of Infrared Beacons for Infrastructure-based Localization." <https://www.youtube.com/watch?v=yDeYZOE0qsk>.